Materials Physics and Mechanics. 2022;48(3): 355-366
Research article
http://dx.doi.org/10.18149/MPM.4832022_6

Submitted: April 19, 2022
Approved: May 4, 2022
Accepted: June 24, 2022

Deformation and mechanical stresses in a magnet with thin-walled quasi-force-free winding

G.A. Shneerson✉, A.V. Khlybov, A.A. Belov, A.P. Nenashev, A.A. Parfentiev, S.A. Shimanskiy

Peter the Great St. Petersburg Polytechnic University, 29 Politechnicheskaya St., St. Petersburg, 195251, Russia

✉ gashneerson@mail.ru

Abstract. The factors leading to an increase in the mechanical stress in the winding of solenoids are considered on the example of a thin-walled magnet with a multi-turn quasi-force-free winding. This example is compared with an ideal system in the form of a solenoid with unlimited length and continuous current distribution. A method for measuring submicron-sized dynamic deformations of the winding in a pulsed field has been developed and verified by comparing experiment results and calculations. Numerical modelling allowed us to distinguish the influence of local edge effects determined by characteristics of the field distribution in the inter-turn gaps. Numerical calculations have shown how the mechanical properties of the material surrounding the coil affect the stress in the winding. The possibility of reducing the stress by increasing Young's modulus of the material was confirmed. The influence on the strength of axial forces that arise near the edges of the turns and lead to compression of the turns in the axial direction is revealed.

Keywords: quasi-force-free magnetic fields, mechanical stresses, local effects, influence of Young's modulus on strength

Acknowledgements. *The work was carried out with the financial support of the Russian Science Foundation, project № 18-19-00230*

Citation: Shneerson GA, Khlybov AV, Belov AA, Nenashev AP, Parfentiev AA, Shimanskiy SA. Research of deformations and strains in a magnet with a thin-walled quasi-forceless winding. *Materials Physics and Mechanics*. 2022;48(3): 355-366. DOI: 10.18149/MPM.4832022_6.

1. Introduction

Generating strong and superstrong magnetic fields remains a challenge due to potential winding failure in magnets, induced by electromagnetic forces. Balanced (quasi-force-free) windings allow for achieving higher magnetic fields without destroying the magnet [1,2]. However, the configurations available for constructing such windings have certain drawbacks lowering their strength characteristics compared to the initial idealized models. The main issues to be resolved to produce magnets with quasi-force-free windings are outlined in [3]. Following the results obtained in [3], this study aims to continue the investigations of mechanical stresses and strains in a real quasi-force-free winding operating in a pulsed magnetic field. Here, this problem is solved for a peculiar magnetic system comprising a thin-walled multi-turn magnet with balanced winding. The stresses arising in the winding placed in

the magnetic field are characterized by the parameter $\eta = 1\mu_0\sigma_M / B_m^2$, which is equal to the ratio of the equivalent mechanical stress (calculated by the formula for the von Mises) to the magnetic pressure of the generated field with the maximum flux density B_m. According to the prototype model of a quasi-force-free magnet, which corresponds to the limiting case when a balanced thin-walled solid winding without gaps has an unlimited length and is placed in a strictly uniform field, this parameter is close to 0.17–0.2 given an arbitrarily small ratio of winding thickness Δ to radius R [2,3]. For reference, this ratio for a single-turn magnet is $R/\Delta >> 1$.

Earlier studies were performed for the simplest magnet with an inner radius of 10 mm and a balanced (quasi-force-free) three-turn winding made of a thin copper band 0.7 mm thick and 11 mm wide [3]. The findings obtained indicate that the arising stresses and strains are affected by the factors taking center stage in the transition from the prototype model mentioned above to a real multi-turn system. One particular factor is the effect of electromagnetic forces due to normal components of the flux density appearing in such a winding. These effects are most pronounced in a solenoid with thin-walled winding. In this paper, we consider deformation in the midplane of a thin-walled winding with a large length-to-diameter ratio. The field is nearly uniform in this region, which allows excluding the influence that transverse components of the magnetic field, caused by the 'integral' effect from the finite length of the solenoid, have on the magnitude and distribution of electromagnetic forces. In this case, the role of the 'local' effect, i.e., the nonuniformity of the field due to inter-turn gaps, is preserved. Estimates of the resulting electromagnetic forces are given in [4]. The second factor affecting the stresses is the reduced mechanical strength of the winding with gaps between the turns compared to the prototype. Previous studies have shown that filling the space adjacent to the winding with a dielectric medium with a sufficiently large Young's modulus not only provides insulation but also increases the stiffness of the mechanical system [2]. The real winding of a multi-turn magnet is a complex multi-component system. Computer simulation allows calculating the strain taking into account the real three-dimensional structure of the magnetic system and finding the value of the strength parameter η. Varying the computational conditions, we can gain the data on the effectiveness of combining the effects of local field nonuniformity and dielectric medium characteristics on the value of the strength parameter. Additional crucial steps are measuring the strain during the discharge and comparing the obtained data with the results of computer simulation. This way, it is possible to assess the suitability of the adopted computational models for describing the deformation in the winding during discharge and estimate the winding's strength characteristics. The calculations can then serve for obtaining comparative estimates of structural parameters of the winding on its strength characteristics.

2. Technique for measuring strain under discharge

There are but scarce studies describing indirect measurements for residual strain in the winding of a multi-turn magnet: by measuring the resistance and inductance after the pulse has stopped in comparison with their initial values [5,6].

Studies on the deformation of magnets with quasi-force-free winding in [7] were carried out using a laser interferometer, recording the boundary displacement in a balanced conductor in the direction of the normal to its surface. These experiments helped identify the characteristics of the quasi-force-free system, for example, the means for adjusting it via an additional external field. However, because the solenoid is displaced during discharge, this method does not allow monitoring of the relative elastic strain and the stresses arising in the conductor. This effect can be eliminated by measuring the strain component tangential to the boundary with a sensor that shifts along with the conductor.

A fiber-optic interferometric sensor, described in [8], has been developed to measure strain. Let us briefly discuss this device. It is a two-arm fiber-optic Mach-Zehnder interferometer. A fiber sensing element is installed in the signal arm of the interferometer so that it is in direct mechanical contact with the measurement sample. The element is a short segment of uncoated optical fiber, glued with slight prestrain to the measurement sample. The sensing elements are equipped with fiber-optic connectors for attaching them to the interferometer. The sensors do not need expensive components and meet all the measurement requirements and conditions: they have a small gauge length, the sensing elements are positioned away from the magnetic system, and are only slightly susceptible to electromagnetic interference during discharge. The sensors allow monitoring of the dynamic displacements in the frequency band up to 100 kHz scale with submicron accuracy. The optical circuit of the device is shown in Fig. 1.

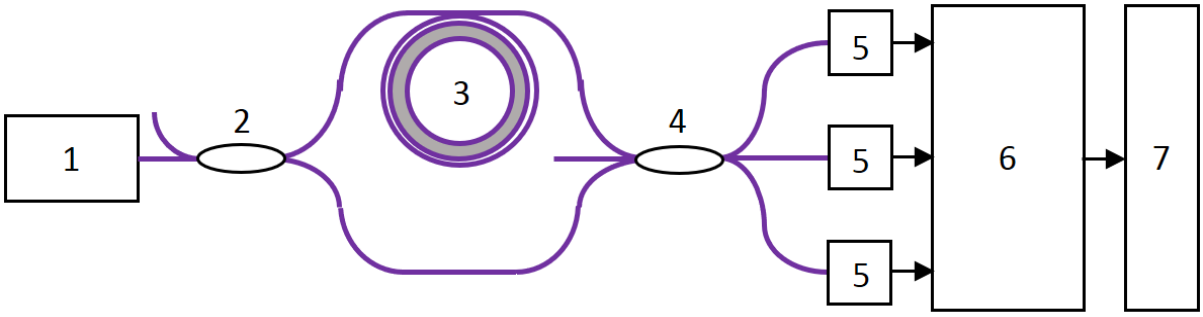

Fig. 1. Schematic of fiber-optic displacement sensor: laser *1*, 2×2 fiber coupler *2*, measurement sample *3*, 3×3 fiber couple *4*, photodetectors *5*, multichannel ADC module *6*, computer *7*

Variations in the length of the sensing element due to deformations of the winding tend to modulate the phase shift between the interfering light waves in accordance with a calculated proportionality constant whose value is determined strictly by the photoelastic properties of the fiber in the sensing element:

$$\Delta l = \delta\varphi \cdot \left[\frac{\lambda}{2\pi n} \cdot \frac{1}{1 - \frac{n^2}{2} \cdot \left(p_{12} - \mu \left(p_{11} + p_{12} \right) \right)} \right]. \quad (1)$$

This formula is obtained from the description of the photoelastic tensor in a strained fiber [9]. Here λ is the wavelength, n is the refractive index of the fiber core at this wavelength, μ is Poisson's ratio determining the elastic properties of the material, p_{11}, p_{12} are the components of the photoelastic tensor of the fiber material (quartz). The expression in braces amounts to $2.158 \cdot 10^{-7}$ m/rad for the given wavelength of 1550 nm.

The optical phase shifts in the arms of the interferometer were calculated numerically based on the data from three detection channels. A symmetric 3×3 fused coupler and a three-channel photodetector were used for this purpose. This technique for phase measurement was first proposed in [10]. The signals of the three detection channels output from the 3×3 coupler, phase-shifted by 120 degrees relative to each other, are extracted and converted to digital simultaneously so that the phase can be determined over a wide frequency band. After a digital low-pass filter is applied to the signals from the detection channels, the time-dependent phase signal can be calculated by the following analytical formula, including the normalization of the signals from the detection channels and differentiation with respect to time, summation of derivatives, and integration over time.

$$\varphi(t)=\int_0^t \frac{u\cdot(\dot{v}-\dot{w})+v\cdot(\dot{w}-\dot{u})+w\cdot(\dot{u}-\dot{v})}{u^2+v^2+w^2}d\tau. \quad (2)$$

Here $u(\tau)$, $v(\tau)$, $w(\tau)$ are time functions that are normalized signals of the detection channels; the overdot denotes the time derivative.

3. Test experiments

The technique was tested by measuring the strain in the sample that was an external electrode of a coaxial system comprising a wire and a thin-walled cylinder. The inner radius of the cylinder was 8 mm, its wall thickness was 0.7 mm. In the ideal case, the test sample is axially symmetric, and the strength of the azimuthal magnetic field at the inner boundary, B_φ, and the magnetic pressure, P_M, are found by simple formulas: $B_\varphi = \mu_0 i/2\pi R$, $P_M = B_\varphi^2/2\mu_0$, where i is current, R is the inner radius of the cylinder. The amplitude and duration of the current pulse were selected so as not to overheat the sample. These conditions are met by a current pulse that is a single half-sine wave with a duration of about 0.6 ms, generated by discharging a capacitor battery. Figure 2 shows current and signal waveforms proportional to the variation in the length of the sensing element (one turn of fiber placed on the outer surface of the cylinder). The data given indicate that the results are well-reproducible, also suggesting a more complex nature of deformation than could be expected from the simplest one-dimensional loading model.

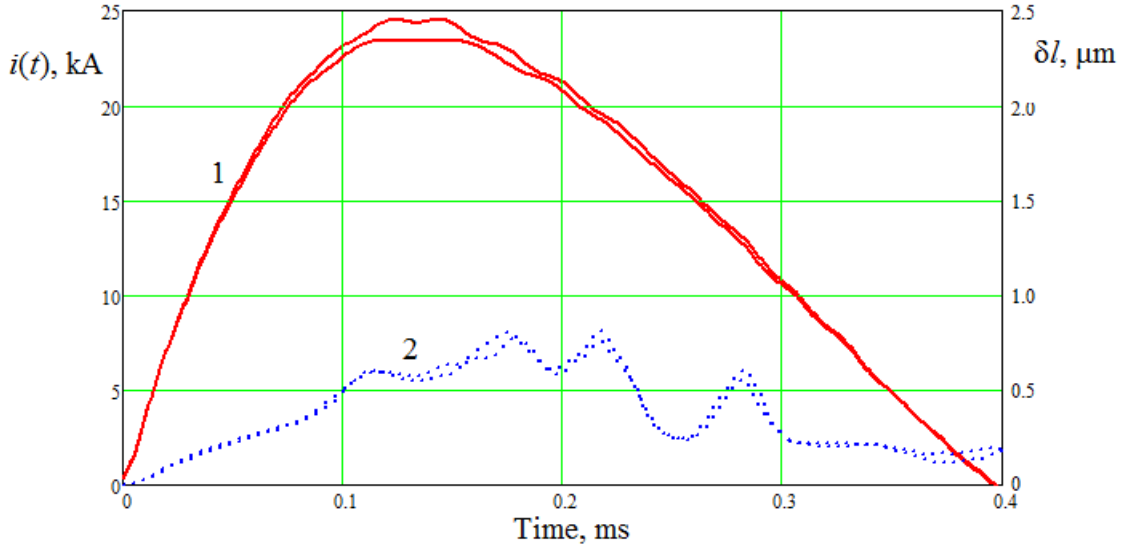

Fig. 2. Current waveform in two experiments with a cylinder (1), variations in the length of the sensing element (2)

The relative strain was calculated based on the data on the elongation measured by the strain gauge. Figure 3 shows the time dependence of relative strain as a function of time for one of the experiments (curve 1). We can conclude from the measurement results that high-frequency components of strain in the cylinder wall are observed in addition to the fundamental mode. These components are generated by higher vibrational modes of the mechanical system, comprising the cylindrical conductor along with its mounting components. The amplitude of these vibrations is relatively small, and their frequency is about 5 times higher than that of the fundamental vibrational mode of the cylinder, which can be estimated by the formula $f \approx (1/2\pi R)\sqrt{E/\gamma}$ where γ is the density of the material, E is the elastic modulus. In our case, $f \approx 7.5\cdot 10^4$ Hz. In view of the above, to identify the fundamental

deformation mode, high-pass filtering of the signal was carried out using a Fourier transform. The corresponding dependence in Fig. 3 (curve 2) gives the strain amplitude value of 15 με. Curve 3 illustrates the results of numerical calculation for relative strain in the axial symmetry approximation. In accordance with the experimental conditions, the calculations assumed one edge of the sample to be rigidly clamped and the other unclamped.

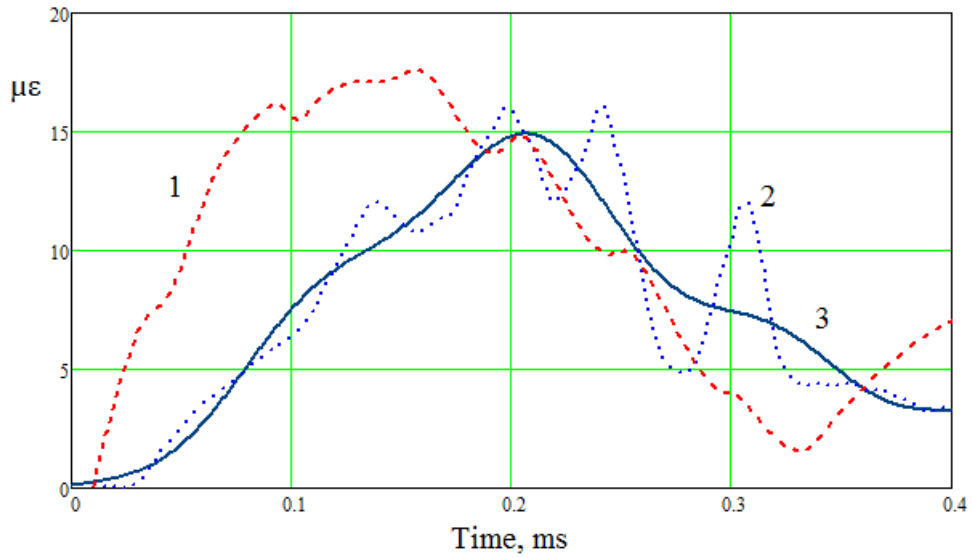

Fig. 3. Relative strain $\Delta R/R$ in cylindrical sample during the test experiment. Result of numerical calculation (*1*), experiment (*2*), experimental data after low-pass filter (*3*)

A certain lag was observed between the times when maximum calculated and measured relative strains were reached in the midplane of the sample. The adopted model proved incapable of explaining the delayed onset of the deformation recorded in the experiments compared to the computational data. The numerical value calculated for the relative strain amplitude is close to the measured one, amounting to 17 με. Thus, despite the existing discrepancies, the measured and calculated maximum strains agree with each other with an accuracy acceptable for estimating the ratio of the amplitude of mechanical stresses to the amplitude of magnetic pressure.

The relative strain amplitude of a thin-walled cylinder can be estimated by a simple formula describing the static loading mode:

$$\varepsilon = \frac{\Delta R}{R} = P_M \frac{R}{d} = \frac{\mu_0 i^2}{8\pi^2 ERd}, \qquad (3)$$

where d is the thickness of the cylinder wall (0.7 mm), E is the elastic modulus of copper (110 GPa), R is the cylinder radius (8 mm). This formula is applicable since the pulse duration (0.6 ms) is tens of times longer than the fundamental vibration period of the tube (about 13 μs). Calculating the relative strain by this formula for a current with an amplitude of 24.4 kA, we obtain the maximum value $\Delta R/R$ = 15.4 με, which is close to the above values. The given formula implies constancy of the relation $q(t) = \varepsilon(t)^{1/2}/i(t)$. The experimental data shown in Fig. 4 indicate that the given ratio changes little for almost the entire duration of the pulse.

The agreement between the calculated and measured values of the strain amplitude was also confirmed in experiments with two samples, where the magnetic system had a configuration identical to the one used in [3]. The winding of the samples consists of three series-connected parts (Fig. 5).

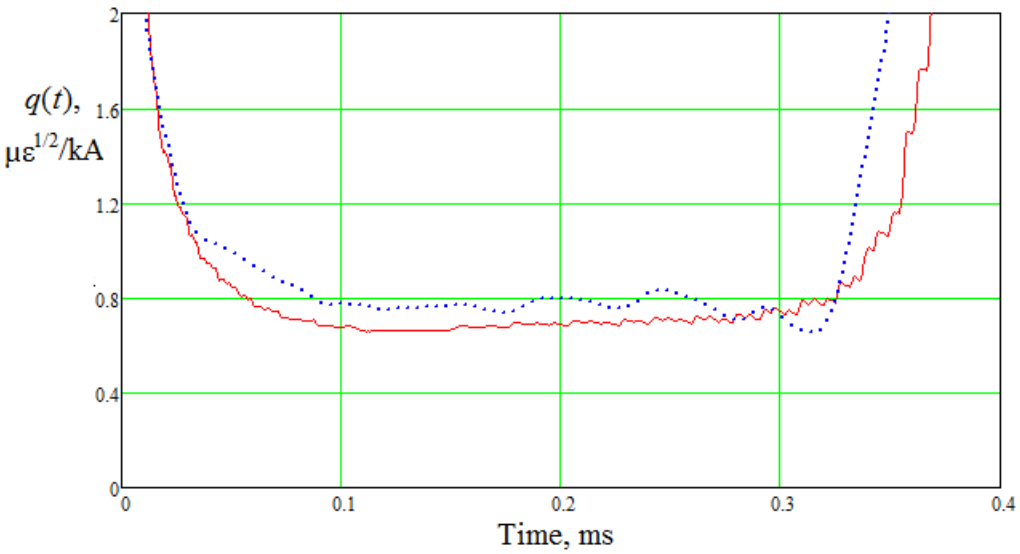

Fig. 4. Dependence $q(t) = \varepsilon(t)^{1/2}/i(t)$ constructed based on the measurements

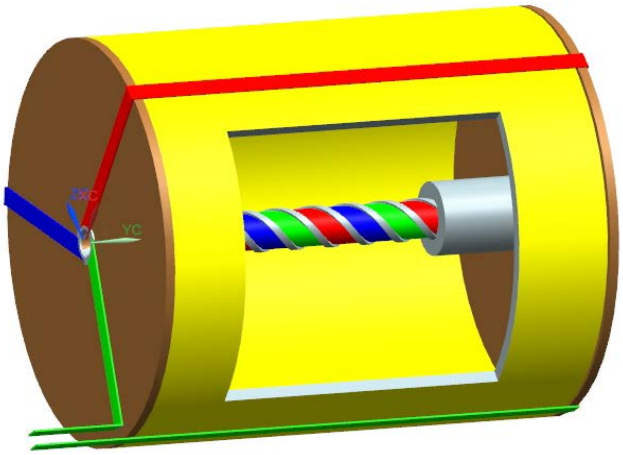

Fig. 5. Schematic of three-turn winding with mounting assembly

Each is made of a copper band 11 mm wide and 0.7 mm thick, placed on a dielectric holder in helical grooves 2 mm deep. Ribs 2 mm wide, securing the conductive band, served as insulating layers between the turns. The experiments were carried out both for uncoated windings (Fig. 6) and for windings impregnated with a layer of dielectric coating (bandage) 3 mm thick, made of epoxy resin with an elastic modulus of about 3.8 GPa (Fig. 7). Figures 6 and 8 show the locations where the strain sensors are attached for samples of both types. The sensors in Type I samples were 30 mm long and were placed directly on the surface of the turns. The sensors (41 mm long) in Type II samples were placed in the slots cut in the filling. Figure 9 shows the current waveforms of the sensor signals in three experiments with Type II samples. The same as in the test experiments, the deformation induced by the vibrations of the mounting assembly was detected after the maximum current. They have little effect on the magnitude of strain amplitude.

Figures 10 and 11 compare the measurements of relative strain and the simulation performed in ANSYS software, taking into account the real three-dimensional configurations of the uncoated sample and the sample with slotted coating. The high-frequency component of strain is also detected in experimental samples appears after reaching the maximum strain and has little effect on its value.

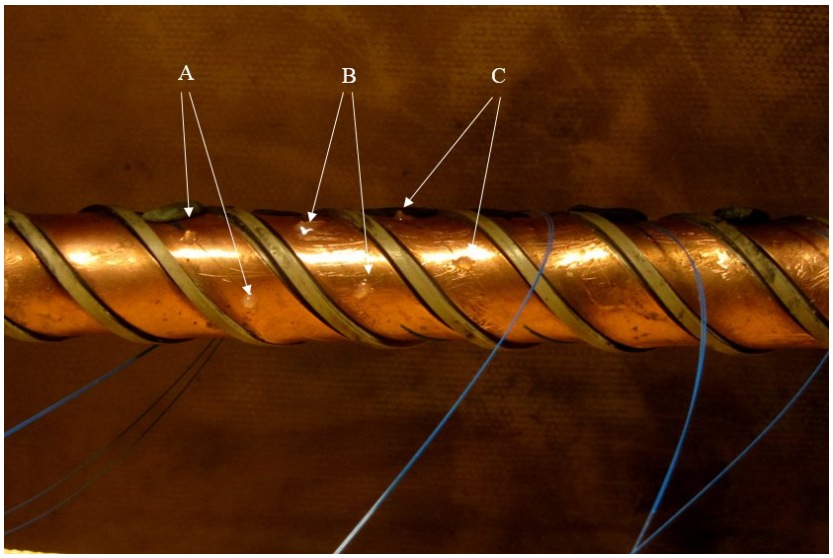

Fig. 6. Type I sample (without a dielectric coating layer). The arrows indicate the locations where copper bands are attached to the tips of glass fiber sensors A, B, C

Fig. 7. Type II sample (winding is coated with a layer of epoxy resin with slots for placing the sensors)

Fig. 8. Arrangement of fiber sensing elements in the slots of the sample with outer coating

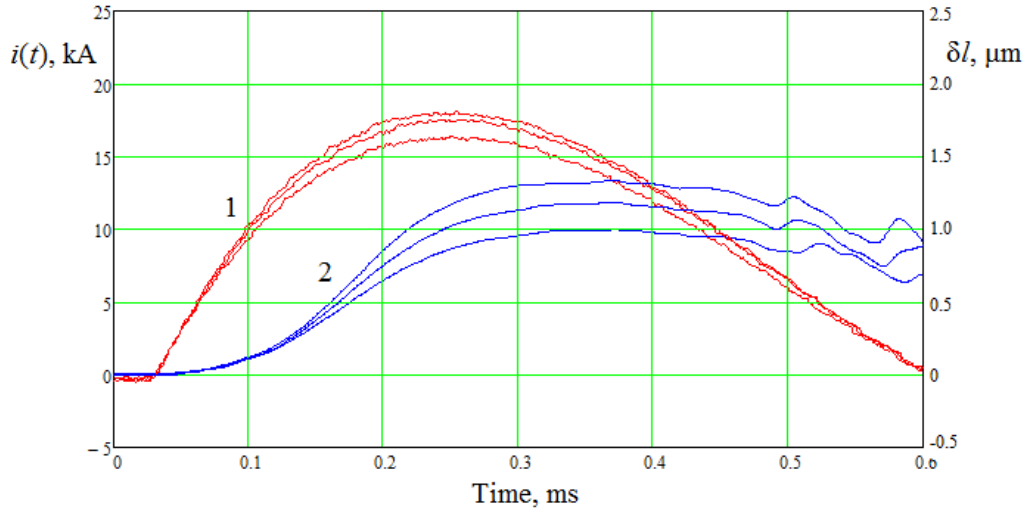

Fig. 9. Current and signal waveforms captured from the strain sensors obtained in three experiments with Type II samples: current (1), displacement, μm (2)

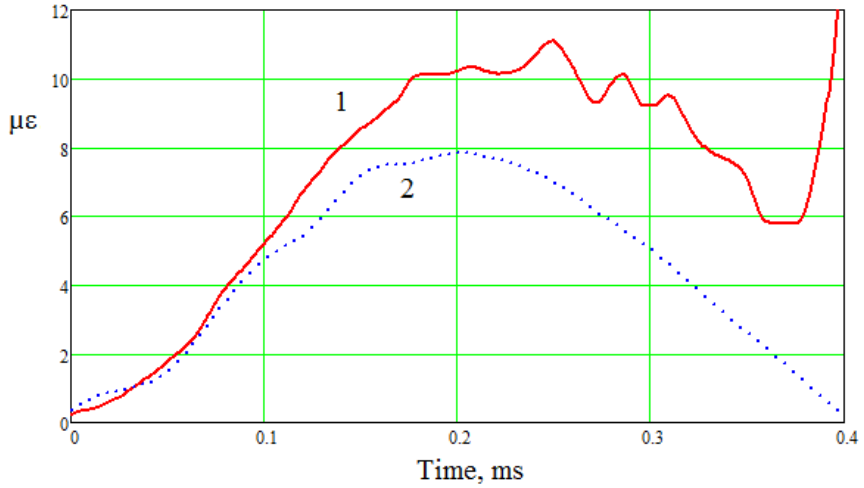

Fig. 10. Comparison of the relative strains measured in Type I samples with the computational results: experiment (1), simulation (2)

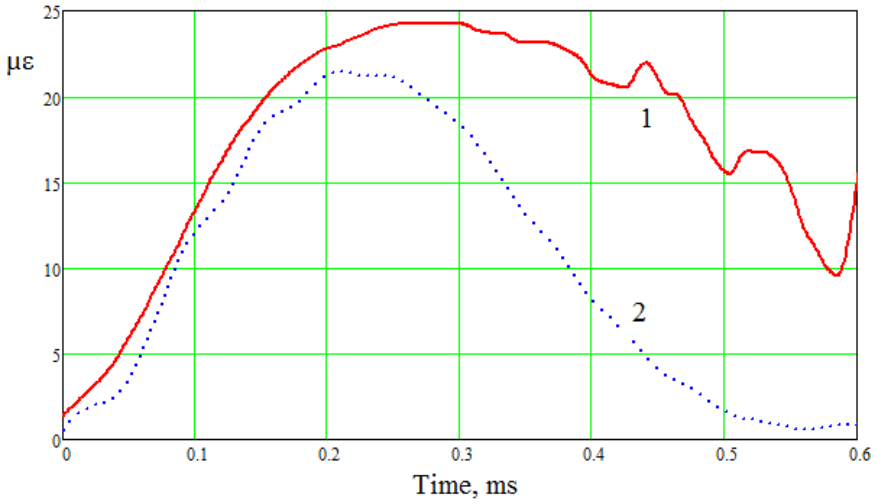

Fig. 11. Comparison of relative strains measured in Type II samples with the computational results: experiment (1), simulation (2)

The discrepancies between the strains measured experimentally and the calculated values appear at the late stage of the discharge. We can safely assume that this is because the three-dimensional computational model is inaccurate in accounting for the mounting assembly of the specimen. The difference between the measured and calculated values of strain amplitude is about 20% for experiments with uncoated specimens, and 8% for experiments with coated specimens.

The goal of the experiments consisted in proving that standard methods of computer simulation are applicable to calculating the stress state of the winding. The calculations allow finding the value of normalized stress η and estimate the flux density at which the equivalent stress exceeds the maximum permissible value, for example, the yield strength of the material. Since this quantity (as well as other strength characteristics of a material subjected to critical pulse loads) itself depends on loading mode, temperature conditions, and other factors, estimating it with an error of 10–20% is acceptable for practical purposes. Benchmarking the data obtained by calculation and experiment, we can argue that the computational models used are well applicable to comparative estimates of normalized stresses in magnets of different configurations. In particular, the results obtained can be used to analyze the effects of 'local' field nonuniformities and parameters of the dielectric medium on mechanical stresses in the winding.

4. Numerical experiments illustrating the character of deformation in thin-walled multi-turn quasi-force-free winding

The initial model of balanced winding in the form of a solid thin-walled cylinder can serve as a starting point for multivariate calculations. The normalized stresses (parameter η) calculated for different configurations are given below. The winding in the first configuration is the same as in the experimental samples and is also clamped only at the edges, but the difference from the prototype model is that no dielectric medium is surrounding the turns. Local field nonuniformities are observed in this system, with no elastic medium increasing the system's stiffness. The factor η in such a magnet amounts to about 40. Its value is given in Table 1 (Row 1); it can be compared with the one for unbalanced winding whose equivalent is a system with longitudinal current, flowing along the axis towards the axial current in the winding and equal to this current. There is no azimuthal field outside the winding in such a system, such that its magnetic pressure would balance the pressure of the poloidal field. The strength parameter reaches the value η = 200.

Table 1. Effect of elastic modulus of the dielectric medium on the mechanical stress in balanced thin-walled winding.

E, GPa	Normalized stress η	
	Δ = 0.7 mm	Δ = 3 mm
No external medium	40	19.5
3.8	4	1.3
10	3	1
20	2	0.83
40	1.4	0.6

Comparing these data, we can see that the stresses in a balanced system are far smaller than in an unbalanced one. However, the inter-turn gaps dramatically reduce the strength of the system compared to the prototype model. Let us now consider the effect of mechanical characteristics of the windings on the stresses. Assuming that the current distribution remains

invariable, we take a system where the gaps between the turns are filled with a non-conductive material with the same elastic modulus as that of the winding material. While the distribution of electromagnetic forces in such a system is the same as in balanced winding with slots not filled with an elastic medium, the influence of gaps on the strength characteristics of the system is excluded. Consequently, the mechanical stresses are reduced by 50 times compared to the system with slots: the normalized stress takes the value $\eta \approx 4$. The transition to a discrete current distribution results in changing the distribution of forces and the nature of the deformation. The deformation of the winding with a thickness of 0.7 mm, magnified by 8400 times, is shown in Fig. 12. The figure shows the influence of axial forces inducing the bending in conductors due to the developing instability. The parameter η increases considerably as a result compared to the value calculated for the prototype model, $\eta = 0.17–0.20$. This result is characteristic of a thin-walled winding with the greatest local nonuniformity of the field and the resulting axial forces. As the winding thickness increases, the axial forces decrease, and the strength of the system against the action of these forces increases. This is confirmed by calculations of mechanical stresses in the winding with turns whose thickness exceeds the thickness of the gap. For example, when the turn thickness increases to 3 mm in a system without a dielectric medium, the parameter η becomes equal to 19.5 instead of 40, and if the gaps are filled with a medium with the same elastic modulus as the winding material, this parameter takes the value $\eta \approx 1.8$.

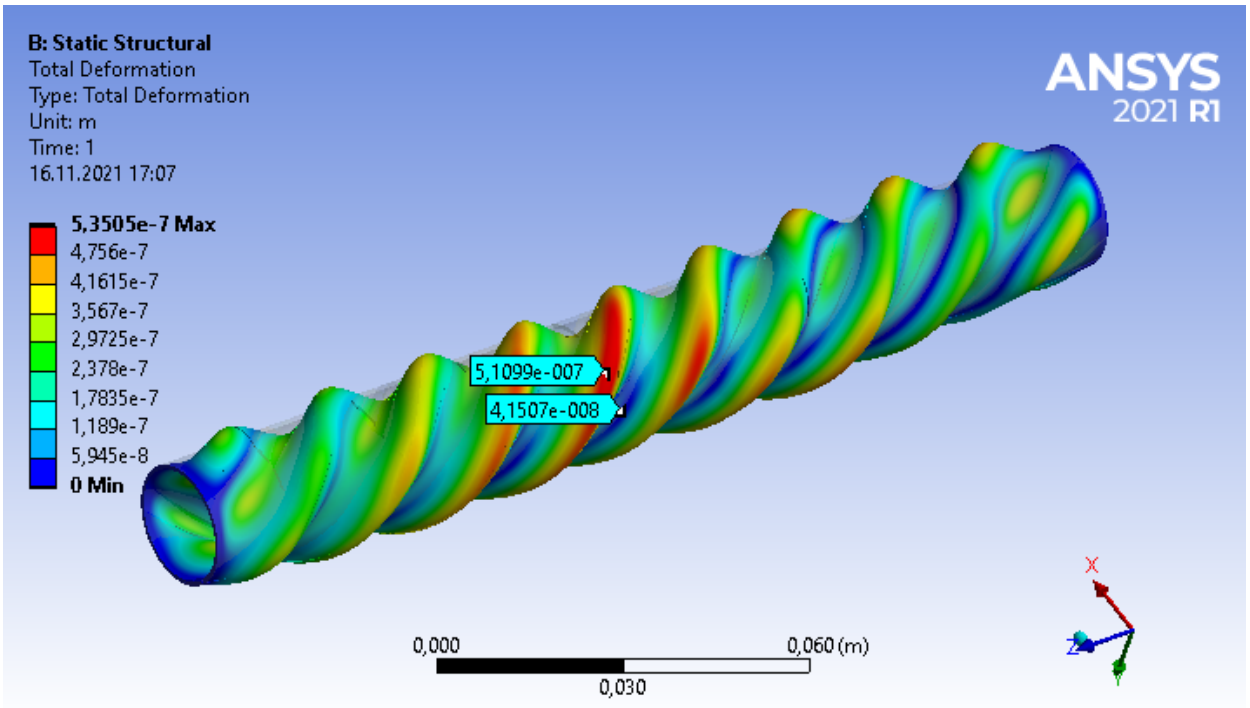

Fig. 12. Qualitative picture of deformation in thin-walled winding under the action of axial forces induced by local nonuniformity of the magnetic field

Windings 11 mm wide with a wall thickness Δ of 0.7 and 3 mm can serve to trace the influence that the elastic modulus of the dielectric medium is used to fill the gaps between the turns and to construct a support cylinder for arranging the winding. An additional part of the system in both examples is an outer bandage 3 mm thick, made of the same material. The table shows the values of normalized mechanical stresses obtained by calculations for magnets with a variable elastic modulus E.

It can be seen from Table 1 that given the same distribution and magnitude of electromagnetic forces, the value of the characteristic parameter decreases sharply for a

medium with an elastic modulus E = 3.8 GPa, typical for epoxy resin, subsequently decreasing to a lesser extent as the elastic modulus of the dielectric medium rises to E = 40 GPa.

5. Conclusion

The technique developed for measuring small strains in the winding in a pulsed field allowed conducting experiments yielding an acceptable agreement between the measured and calculated strains in a thin-walled magnet with balanced winding. Simulations of mechanical stresses in the system confirmed the expected influence of the factors leading to an increase in stress compared to an ideal system in the form of a solenoid with unlimited length and a continuous current distribution. The role of normal components of the magnetic field, caused by local edge effects in the vicinity of inter-turn gaps and generating longitudinal forces, has been described for a magnet with thin-walled winding. This effect is important since it also preserves its magnitude in systems where the appearance of such components is excluded in the integral picture of the field. Moreover, we have considered the influence that the characteristics of the medium filling the inter-turn gaps have on the stresses in the winding, establishing that normalized stresses close to unity can be achieved in a balanced single-layer multi-turn winding with an increasing elastic modulus of this medium.

References

1. Shneerson GA, Koltunov OS, Khozikov VYu. Minimizatsiya ostatochnykh napryazheniy v magnitnykh sistemakh s kvazibessilovym raspredeleniyem toka. *ZhTF*. 2002;72(1): 110-116. (in Russian)
2. Shneerson G, Dolotenko M, Krivosheev S. *Strong and Superstrong Pulsed Magnetic Fields Generation*.De Gruyter, Berlin; 2014.
3. Shneerson ., Nenashev P, Parfentiev A, Vecherov I,Shimanskiy S. Problems and Possible Ways of Achieving the Design Strength of Quasi-Force-Free Windings. *IEEE Transactions on Plasma Science*. 2018;46(9): 3209-3213.
4. Shneerson G, Krivosheev S, Magazinov S. Electromagnetic Forces Acting on Thin Flat Conductors of Pulse Power Equipment. *IEEE Transactions on Plasma Science*. 2021;49(7): 2148-2152.
5. Jones H, Herlach F, Lee J et al. 50 tesla pulsed magnets using a copper conductor externally reinforced with stainless steel. *IEEE Trans. on Magnetics*. 1988;24(2): 1055-1058.
6. Portugall G, Mainson M, Billlete J, Lecouturier F, Frings P, Rikken GLJA. Towards 100T-Europian Activites in the Development of Non-Destructive Pulsed Magnet. XI Megagauss Conference, Ed. I.R. Smith and B.M. Novac, 2006, London, pp. 53-57.
7. Shneerson G, Koltunov O, Berezkin A, Vecherov I, Krivosheev S, Nenashev A, Parfentiev A. Development and Invesnigation of One-LayerQuasi-Force-Free Magnets // XIV Megagauss Conference, Ed. G.F.Kiuttu, K.W.Struve and J. H.Degnan, 2012, Maui, pp. 46-50.
8. Khlybov AV, Belov AA, Nenashev AP, Shneerson GA, Shimanskiy SA. Measurement of Coil Deformation in Pulsed High Magnetic Field Using a Fiber Optic Interferometer // 2020 IEEE International Conference on Electrical Engineering and Photonics (EExPolytech), St. Petersburg, Russia, 2020, pp. 255-257.
9. Becker T, Ziemann O, Engelbrecht R, Schmauss B. Optical Strain Measurement with Step-Index Polymer Optical Fiber Based on the Phase Measurement of an Intensity-Modulated Signal. *Sensors*. 2018;18(7): 2319.
10. Koo KP, Tveten AB, Dandridge A. Passively stabilized fiber interferometers using 3x3 fiber directional couplers. *Appl. Phys. Lett*. 1982;41: 616.

THE AUTHORS

Shneerson G.A.
e-mail: gashneerson@mail.ru
ORCID: 0000-0002-7087-098X

Khlybov A.V.
e-mail: a.khlybov@spbstu.ru
ORCID: 0000-0003-4457-7816

Belov A.A.
e-mail: belov@spbstu.ru
ORCID: 0000-0003-0617-4514

Nenashev A.P.
e-mail: nenashev_ap@spbstu.ru
ORCID: -

Parfentiev A.A.
e-mail: -
ORCID: -

Shimanskiy S.A.
e-mail: s.a.shimanskiy@gmail.com
ORCID: -